

# UC Irvine

## UC Irvine Previously Published Works

### Title

Unusual diffusive effects on the ESR of Nd<sup>3+</sup> ions in the tunable topologically nontrivial semimetal YBiPt

### Permalink

<https://escholarship.org/uc/item/3f86w9xc>

### Journal

Journal of Physics Condensed Matter, 28(12)

### ISSN

0953-8984

### Authors

Lesseux, GG  
Garitezi, TM  
Rosa, PFS  
[et al.](#)

### Publication Date

2016-03-31

### DOI

10.1088/0953-8984/28/12/125601

### Copyright Information

This work is made available under the terms of a Creative Commons Attribution License, available at <https://creativecommons.org/licenses/by/4.0/>

Peer reviewed

# Unusual diffusive effects on the ESR of $\text{Nd}^{3+}$ ions in the tunable topologically nontrivial semimetal YBiPt

G G Lesseux<sup>1</sup>, T M Garitezi<sup>1</sup>, P F S Rosa<sup>1,2</sup>, C B R Jesus<sup>1</sup>, S B Oseroff<sup>3</sup>, J L Sarrao<sup>4</sup>, Z Fisk<sup>2</sup>, R R Urbano<sup>1</sup>, P G Pagliuso<sup>1</sup> and C Rettori<sup>1,4</sup>

<sup>1</sup> Instituto de Física ‘Gleb Wataghin’, UNICAMP, Campinas, SP 13083-859, Brazil

<sup>2</sup> University of California, Irvine, CA 92697-4573, USA

<sup>3</sup> San Diego State University, San Diego, CA 92182, USA

<sup>4</sup> Los Alamos National Laboratory, Los Alamos, NM 87545, USA

<sup>5</sup> CCNH, Universidade Federal do ABC (UFABC), Santo André, SP 09210-580, Brazil

E-mail: [lesseuxgg@gmail.com](mailto:lesseuxgg@gmail.com)

Received 26 October 2015, revised 9 January 2016

Accepted for publication 12 January 2016

Published 24 February 2016




CrossMark

## Abstract

Electron spin resonance (ESR) of diluted  $\text{Nd}^{3+}$  ions in the *topologically nontrivial* semimetallic (TNSM) YBiPt compound is reported. The cubic YBiPt compound is a non-centrosymmetric half Heusler material which crystallizes in the  $F43m$  space group. The low temperature  $\text{Nd}^{3+}$  ESR spectra showed a  $g$ -value of 2.66(4) corresponding to a  $\Gamma_6$  cubic crystal field Kramers’ doublet ground state. Remarkably, the observed metallic and diffusive (Dysonian)  $\text{Nd}^{3+}$  lineshape presented an unusual dependence with grain size, microwave power,  $\text{Nd}^{3+}$  concentration and temperature. Moreover, the spin dynamic of the localized  $\text{Nd}^{3+}$  ions in YBiPt was found to be characteristic of a *phonon-bottleneck* regime. It is claimed that, in this regime for YBiPt, phonons are responsible for mediating the diffusion of the microwave energy absorbed at resonance by the  $\text{Nd}^{3+}$  ions to the thermal bath throughout the skin depth ( $\delta \simeq 15 \mu\text{m}$ ). We argue that this is only possible because of the existence of highly mobile conduction electrons inside the skin depth of YBiPt that are strongly coupled to the phonons by spin–orbit coupling. Therefore, our unexpected ESR results point to a coexistence of metallic and insulating behaviors within the skin depth of YBiPt. This scenario is discussed in the light of the TNSM properties of this compound.

Keywords: topological materials, electron spin resonance, half-Heusler compound

 Online supplementary data available from [stacks.iop.org/JPhysCM/28/125601/mmedia](http://stacks.iop.org/JPhysCM/28/125601/mmedia)

(Some figures may appear in colour only in the online journal)

## 1. Introduction

The recognition of a new quantum state of matter in topological insulating (TI) materials has recently attracted a great deal of attention from the condensed matter scientific community [1–5]. Nontrivial topological invariants in gapped bulk electronic bands yield robust gapless conducting states on the surface (edges) of these materials. Such conducting states protected by time-reversal symmetry emerge as consequence

of an inverted band gap due to strong spin–orbit (SO) coupling [6, 7]. Moreover, the underlying physics of these materials is intimately connected to the quantum spin Hall effects (QSHE) [1, 8]. Quantum wells of HgTe/CdTe [9, 10] were confirmed as a bi-dimensional (2D) TI material. Yet  $\text{Bi}_{1-x}\text{Sb}_x$  alloys [11, 12] and the tetradymite semiconductors such as  $\text{Bi}_2\text{Se}_3$ ,  $\text{Bi}_2\text{Te}_3$  and  $\text{Sb}_2\text{Te}_3$  [13–15] are considered 3D TIs. A distinct class called topological crystalline insulators (TCI) [16] is realized in SnTe [17] and  $\text{Pb}_{1-x}\text{Sn}_x\text{Se}$  [18]. In this

specific case, the surface metallic states with locked spin and momentum are protected by structural crystalline symmetries rather than the time-reversal one. Besides these well established TIs and TCIs, some Kondo insulator compounds, such as YbBiPt [19–21], SmB<sub>6</sub> [22–27] and YbB<sub>6</sub> [28] were also recently suggested as topological Kondo insulators (TKI). It is worth emphasizing that strong SO coupling is a crucial ingredient in all of these materials [20, 29, 30].

In particular, for the rare earth (RE) series of non-centrosymmetric half Heusler ternary semiconducting/semimetallic REBiPt compounds, first principle calculations predict band inversion in many members of this family. The topological (gapless) metallic surface states may emerge by either applying strain or chemical pressure [19, 31, 32]. These materials behave as small gap semiconductors ( $\Delta \gtrsim 10$  meV) in the bulk with robust protected metallic states on the surface due to their strong SO coupling and nontrivial  $Z_2$  topology [19, 31, 32].

Among the REBiPt compounds, YBiPt has gained distinguished attention as a nontrivial topological semimetal due to its unusual transport properties [33] and the presence of conducting surface states [34]. Despite still being controversial [35], superconductivity with transition temperature  $T_c \simeq 0.77$  K has been reported for YBiPt [34, 36]. Regardless of its inconclusive nature, the superconducting phase associated with nontrivial topology of the electronic bands might, in principle, create a propitious framework to investigate the putative surface states known as Majorana fermions [4, 37, 38].

Electron spin resonance (ESR) of diluted REs is a powerful local technique that can directly probe the nature of the interactions between localized magnetic moments and their electronic environment as well as the local, dynamic and static, crystalline site symmetry [39–41]. Therefore, ESR may be a suitable tool to investigate the robust metallic states in *topologically nontrivial* materials. In this regard, our research group studied the crystalline electric field (CEF) effects of diluted REs (Nd<sup>3+</sup>, Gd<sup>3+</sup> and Er<sup>3+</sup>) in Y<sub>1-x</sub>RE<sub>x</sub>BiPt about 15 years ago [42, 43]. At that time, we found an intriguing and anomalous Nd<sup>3+</sup> ESR lineshape behavior in Y<sub>1-x</sub>Nd<sub>x</sub>BiPt, which has not been reported because its nature was unrelated to CEF effects. Nonetheless, enlightened by the advent of TI materials and their astonishing physical properties recently discovered in these systems, we revisited this new subject and carried out new ESR experiments in order to elucidate the origin of such unusual lineshape behavior.

Therefore, in this work we report a detailed ESR investigation of the Nd<sup>3+</sup> lineshape in Y<sub>1-x</sub>Nd<sub>x</sub>BiPt ( $0.002 \lesssim x \lesssim 0.10$ ). Our results provide important evidence of highly mobile (Dirac-like) conduction electrons (*ce*) strongly coupled, via SO-coupling, to the phonons within the microwave skin depth of YBiPt. Our main findings are: (i) coexistence of metallic and insulating behaviors (i.e. low carrier semimetallic behavior) within a microwave skin depth of  $\delta \simeq 15$   $\mu$ m (considered a bulk measurement in conventional metallic systems [40, 41]); (ii) unusual microwave power, particle size, Nd<sup>3+</sup> concentration and temperature dependence revealed by spectral analysis; and (iii) occurrence of a *phonon-bottleneck*

relaxation process in Nd<sup>3+</sup> doped YBiPt. All these features are discussed in light of the *topologically nontrivial* semimetallic (TNSM) properties of this compound.

## 2. Experimental details

Several batches of Y<sub>1-x</sub>Nd<sub>x</sub>BiPt ( $0.002 \lesssim x \lesssim 0.10$ ) were synthesized using the self-flux technique [44] with starting composition (1-x)Y:xNd:1Pt:20Bi. High-purity (99.99%) RE elements from Ames have been used. The crucible containing the elements was placed in a quartz tube sealed in vacuum and slowly heated up to 1170 °C. After being kept at this temperature for 2h, the tube was cooled down to 900 °C with a rate of 10 °C h<sup>-1</sup>. The collected crystals have as-grown planes with dimensions up to 4 × 4 mm<sup>2</sup>. X-ray powder diffraction was used to verify the cubic crystalline structure and F43 *m* space group of YBiPt.

The x-band ( $\nu \simeq 9.4$  GHz) ESR experiments were carried out in a conventional CW Bruker-ELEXSYS 500 spectrometer using 100 kHz magnetic field modulation and a TE<sub>102</sub> cavity coupled to an Oxford helium gas flow system and a quartz/stainless steel cold tail liquid helium dewar. The ESR spectra were taken between  $\approx 2$   $\mu$ W and  $\approx 200$  mW of microwave power. The 1.6 K ESR spectra were performed in a conventional Varian ESR spectrometer using a TE<sub>102</sub>. The sample temperature was controlled using a quartz tail dewar for pumped liquid-helium bath experiments. To verify the appropriate performance of our AFC circuitry in the microwave power dynamic range, we have carried out ESR experiments of Er doped Au under the same experimental conditions used in this work (see figure 1 of supplementary information, [stacks.iop.org/JPhysCM/28/125601/mmedia](http://stacks.iop.org/JPhysCM/28/125601/mmedia)).

All ESR experiments were performed on gently powdered Y<sub>1-x</sub>Nd<sub>x</sub>BiPt single crystals with  $0.002 \lesssim x \lesssim 0.10$  and selected grain sizes within  $\simeq 100$   $\mu$ m to  $\simeq 2$  mm. The average ratio between grain size and skin depth is  $\lambda = d/\delta \gtrsim 6.6$ . The skin depth  $\delta = (\rho/\pi\nu\mu_r\mu_o)^{1/2} \simeq 15$   $\mu$ m was estimated taking into account  $\nu = 9.4$  GHz and the resistivity value of YBiPt at low-*T* from [34]. We should mention here that at 10% Nd impurity doping the overall *T* dependence of the resistivity behavior remains similar to the undoped YBiPt. One can only observe a slight change in the residual resistivity, which is basically comparable with that found for crystals of the same compound coming from distinct batches. It should be mentioned that this level of doping is still away from the percolation limit if one considers the cubic crystalline structure symmetry.

## 3. Experimental results

First of all it is reasonable and quite convenient to introduce here the framework necessary to analyze the ESR lineshape behavior in Y<sub>1-x</sub>Nd<sub>x</sub>BiPt. It is well known that the microwave electromagnetic field is attenuated on the surface of metals due to their high conductivity. Thus, the microwave only penetrates the material up to a small length scale called *skin depth*,  $\delta$ , which is usually much smaller than the sample

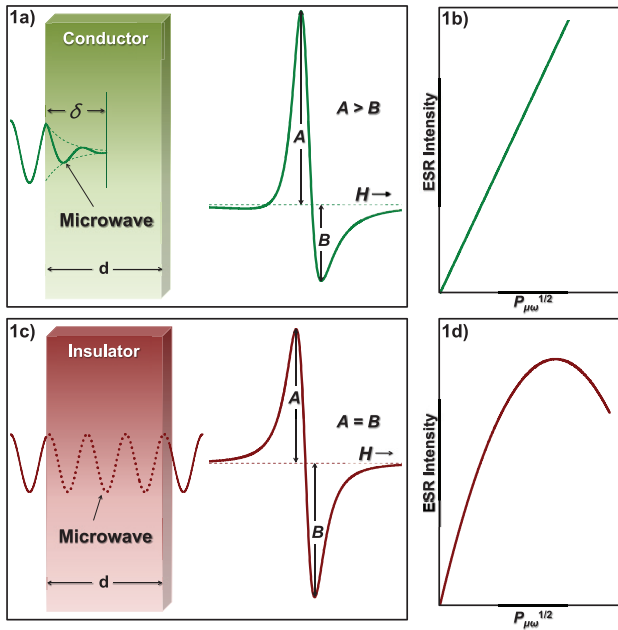


**Figure 1.** (a) and (b) illustrate the microwave penetration and ESR lineshape; (c) and (d) represent the microwave power dependence of the ESR signal intensity in metallic and insulating samples, respectively. A maximum in the intensity as depicted in (d) is expected for homogeneous and non-ideal inhomogeneous broadening cases [46].

dimensions. This fact leads to a vertically asymmetric ESR lineshape named Dysonian (figure 1(a)) [45]. In a metal, a local moment spin system has a very fast relaxation process which allows the resonating spins to transfer the absorbed microwave energy to the lattice very rapidly via exchange interaction with the *ce*. As such, the ESR signal intensity (doubly integrated ESR spectrum) usually increases linearly as a function of (microwave power)<sup>1/2</sup> at a given temperature, as illustrated in figure 1(b). In contrast, the resonating spins present a symmetric ESR lineshape called Lorentzian when the microwave goes through the entire volume of an insulating material, as shown in figure 1(c). As the insulating materials are free of *ce*, the relaxation mechanism is dominated by phonons which are much slower than those in a metal. As a consequence, the ESR signal intensity in an insulator can saturate at high microwave power when the population of the spin levels, split by the Zeeman effect, tends to be equal at a given temperature. This effect is displayed in figure 1(d).

In fact, the overall ESR lineshape in a metallic environment is usually analyzed by the well accepted approach given by Dyson's theory. In particular, the ESR lineshape for the microwave absorption at resonance by a localized magnetic ion is described in the diffusionless limit,  $1 \leq A/B \lesssim 2.6 \rightarrow T_D/T_2 \gg 1$  [45, 47], where  $T_D$  is the average time that a resonant spin takes to diffuse across the skin depth and  $T_2$  is the spin-spin transverse relaxation time. Within this limit, Dyson's theory can be approximately simulated by a simple admixture of absorption and dispersion of Lorentzian lineshapes [48] with the  $A/B$  ratio changing monotonically from  $A/B \approx 1$  to  $A/B \approx 2.6$  for sample size  $d$  smaller and larger than  $\delta$ , respectively [45, 47–49]. Nonetheless, this simple and fortuitous artificial

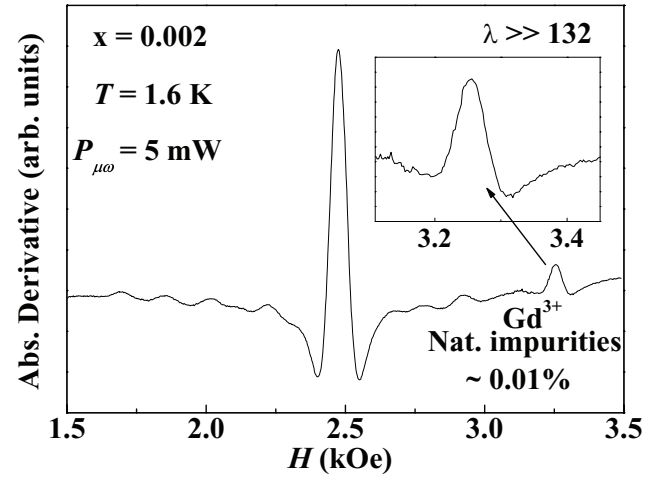


**Figure 2.** ESR spectrum of  $Y_{1-x}Nd_xBiPt$  for  $x = 0.002$  and natural  $Gd^{3+}$  impurities at  $T = 1.6$  K,  $P_{\mu\omega} \approx 5$  mW and  $\lambda \gg 132$ . The inset shows the ESR lineshape for  $Gd^{3+}$ .

mathematics is commonly used to simulate the observed resonance lineshapes and it has to be shown to give similar results as the correct equations given by Feher and Dyson [45, 47]. Nevertheless, when  $A/B$  exceeds 2.6, Dyson's theory anticipates the presence of diffusive effects,  $A/B \gtrsim 2.6 \rightarrow T_D/T_2 \lesssim 1$ , (figure 7 from [45]) [45, 47]. This means that the resonating spins diffuse across the skin depth with a diffusion time  $T_D$  comparable to the spin-spin relaxation time,  $T_2$ .

Therefore, following the ideas given above equation (1) gives the derivative of the admixture of absorption ( $\chi''$ ) and dispersion ( $\chi'$ ) of Lorentzian lineshapes,

$$\frac{d[(1-\alpha)\chi'' + \alpha\chi']}{dH} = \chi_0 H_0 \gamma^2 T_2^2 \left[ \frac{2(1-\alpha)x}{(1+x^2+s)^2} + \frac{\alpha(1-x^2+s)}{(1+x^2+s)^2} \right] \quad (1)$$

$$x = (H_0 - H)\gamma T_2$$

where  $H_0$  and  $H$  are the resonance and the applied magnetic fields, respectively,  $\gamma$  is the gyromagnetic ratio,  $T_2$  is the spin-spin relaxation time,  $\alpha$  is the admixture parameter of absorption ( $\alpha = 0$ ) and dispersion ( $\alpha = 1$ ), and  $\chi_0$  is the paramagnetic contribution from the static susceptibility.

In the following, the analysis of the resonance lineshape also takes into account the saturation term  $s = \gamma^2 H_1^2 T_1 T_2$  which has been phenomenologically introduced in equation (1).  $H_1$  is the strength of the microwave magnetic field and  $T_1$  is the spin-lattice relaxation time [39].

Figure 2 presents the ESR spectra of  $Nd^{3+}$  in  $Y_{1-x}Nd_xBiPt$  for  $x = 0.002$  as well as the natural  $Gd^{3+}$  impurities ( $\lesssim 100$  ppm for the Y 4N) at  $T = 1.6$  K and microwave power of  $P_{\mu\omega} \approx 5$  mW for  $\lambda \gg 132$ . At a glance one can easily observe a striking and unexpected result: the ESR lineshape for  $Gd^{3+}$  impurities is a metallic-like (Dysonian) close to the diffusionless-like regime ( $A/B \approx 2.7 \rightarrow T_D/T_2 \gtrsim 1$ ), while that of the  $^{140}Nd^{3+}$  ( $I = 0$ ) presents a completely diffusive lineshape ( $A/B \approx 5 \rightarrow T_D/T_2 \approx 0.4$ ) [45, 47]. This is an apparent paradox because both REs are localized magnetic moments diluted in

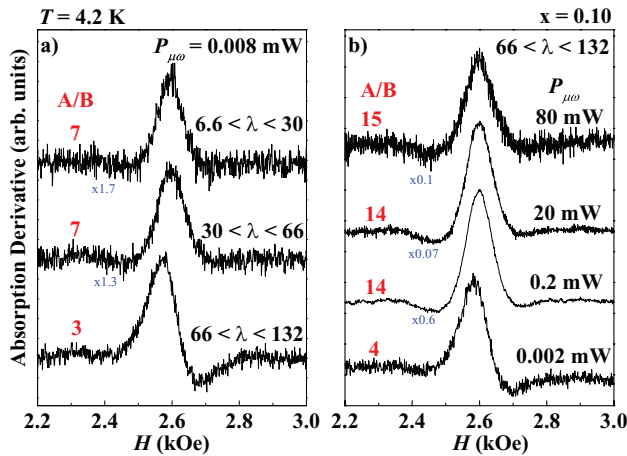


**Figure 3.**  $\text{Nd}^{3+}$  ESR lineshape of  $\text{Y}_{0.9}\text{Nd}_{0.1}\text{BiPt}$  at  $T = 4.2$  K as a function of (a) particle size  $6.6 \lesssim \lambda \lesssim 132$  at fixed  $P_{\mu\omega} \approx 8 \mu\text{W}$  and (b)  $P_{\mu\omega}$  with particle size  $66 \lesssim \lambda \lesssim 132$ . The spectra scaling factors are indicated in blue.

the very same site in the material. Moreover, except for their distinct concentrations and Russell–Saunders ( $L - S$ ) coupling, both magnetic probes are under the same experimental conditions, i.e.  $T$ ,  $P_{\mu\omega}$  and particles size much larger than the skin depth.

Figure 3(a) shows the ESR spectra of  $\text{Y}_{1-x}\text{Nd}_x\text{BiPt}$  for  $x = 0.10$  at  $T = 4.2$  K,  $P_{\mu\omega} \approx 8 \mu\text{W}$ , and  $6.6 \lesssim \lambda \lesssim 132$ . Remarkably, it is clear from these data that the observed change of the lineshape, going from  $A/B \approx 3$  for large particles to  $A/B \approx 7$  for smaller particles, does not correspond to the  $A/B$  values expected from Dyson’s theory for diffusionless ESR lineshape ( $1 \lesssim A/B \lesssim 2.6$ ). Instead, the lineshape of the smaller particles presents a strong diffusive shape,  $A/B \approx 7 \rightarrow T_D/T_2 \approx 0.2$ , despite the fact that the particle size is still larger than the skin depth  $\delta$ . Figure 3(b), in turn, presents the  $P_{\mu\omega}$  dependence of the ESR lineshape for the  $66 \lesssim \lambda \lesssim 132$  sample. These data show that the ESR lineshape is closer to the diffusionless limit ( $A/B \approx 4 \rightarrow T_D/T_2 \approx 0.9$ ) at very low power ( $\approx 2 \mu\text{W}$ ). However, by increasing  $P_{\mu\omega}$  up to  $\approx 200 \mu\text{W}$  the lineshape becomes completely diffusive ( $A/B \approx 14 \rightarrow T_D/T_2 \approx 0.02$ ). Yet, up to this power level the doubly integrated ESR spectra grow linearly with  $[P_{\mu\omega}]^{1/2}$  showing no saturation effects (not shown). Again, these results add up to contrasting behavior displayed by the ESR lineshape of localized magnetic moments in this material. By further increasing  $P_{\mu\omega}$ , the lineshape remains diffusive and the doubly integrated spectra begin to display saturation effects above  $\approx 5$  mW (see figure 6(b) below), confirming the absorption character of the diffusive resonance lineshape.

Figures 4(a)–(c) display the  $P_{\mu\omega}$  dependence of the ESR lineshape of  $\text{Y}_{1-x}\text{Nd}_x\text{BiPt}$  for  $x = 0.002$ , 0.005 and 0.10, respectively, with  $6.6 \lesssim \lambda \lesssim 30$  at  $T = 4.2$  K. These results show that our smallest particles present almost diffusionless lineshapes ( $A/B \approx 2.2 - 2.5 \rightarrow T_D/T_2 \gg 1$ ) at low concentration (figure 4(a)) and strong diffusive lineshapes ( $A/B \approx 9 - 17 \rightarrow T_D/T_2 \approx 0.10 - 0.01$ ) at high concentration (figure 4(c)), both nearly independent of  $P_{\mu\omega}$ . Nonetheless, the lineshape presents a dramatic and unusual change between

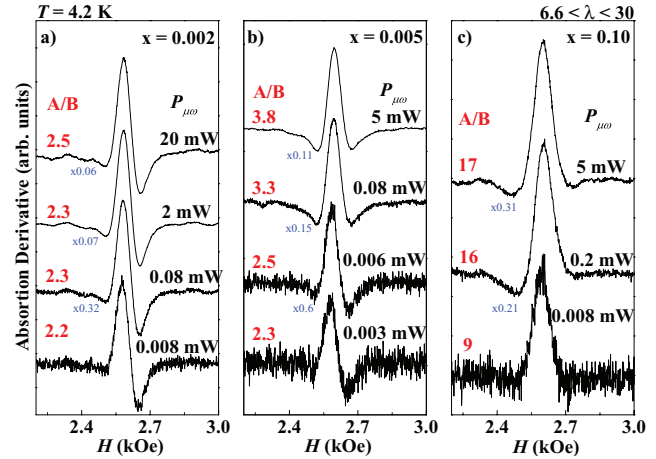


**Figure 4.**  $P_{\mu\omega}$  dependence of the ESR lineshape of  $\text{Y}_{1-x}\text{Nd}_x\text{BiPt}$  with  $6.6 \lesssim \lambda \lesssim 30$  at  $T = 4.2$  K for: (a)  $x = 0.002$ , (b)  $x = 0.005$  and (c)  $x = 0.10$ . The spectra scaling factors are indicated in blue.

these two regimes for intermediate concentrations, e.g.  $x = 0.005$  in figure 4(b) (also see figure 3(b)). This sample shows a diffusionless ESR lineshape ( $A/B \approx 2.3 \rightarrow T_D/T_2 \gg 1$ ) with low  $P_{\mu\omega} \approx 3 \mu\text{W}$  although its lineshape becomes noticeably more diffusive ( $A/B \approx 3.3 \rightarrow T_D/T_2 \approx 0.9$ ) upon increasing  $P_{\mu\omega}$  up to an intermediate value of about  $80 \mu\text{W}$ . Yet, up to these power levels, the ESR spectra do not show saturation effects (e.g. saturation of ESR intensity). By further increasing  $P_{\mu\omega}$ , the lineshape remains diffusive and the ESR intensity (doubly integrated spectra) saturates at higher power levels, similarly to the data presented in figures 6(a) and (b), confirming again the absorption character of the diffusive resonance lineshape.

Figures 5(a)–(c) present the  $T$  dependence of the ESR lineshape of  $\text{Y}_{1-x}\text{Nd}_x\text{BiPt}$  with  $6.6 \lesssim \lambda \lesssim 30$  for  $x = 0.002$  at  $P_{\mu\omega} \approx 5$  mW,  $x = 0.005$  at  $P_{\mu\omega} \approx 5$  mW and  $x = 0.10$  at  $P_{\mu\omega} \approx 0.2$  mW, respectively. These results show that at  $T \lesssim 10$  K the ESR lineshape displays strong diffusive character. The increase of  $T$  tends to restore the ESR lineshape in the diffusionless regime ( $A/B \approx 2 - 4$ ) as observed at low- $P_{\mu\omega}$  for large particles (see figures 3(a) and (b)).

Figures 6(a) and (b) display the  $P_{\mu\omega}$  and  $T$  dependence of the ESR intensity of  $\text{Y}_{1-x}\text{Nd}_x\text{BiPt}$  with  $6.6 \lesssim \lambda \lesssim 30$  for  $x = 0.002$  and 0.10, respectively. Similar results were obtained for  $x = 0.005$  and  $x = 0.05$  (not shown). Notice that the resonance intensity for  $x = 0.10$  also saturates above  $\approx 5$  mW in spite of its diffusive-like lineshape; again, confirming the absorption character of the diffusive resonance lineshape. We may thus conclude that the ensemble of  $\text{Nd}^{3+}$  ions in  $\text{Y}_{1-x}\text{Nd}_x\text{BiPt}$  ( $0.002 \lesssim x \lesssim 0.10$ ) saturates as  $P_{\mu\omega}$  increases and  $T$  decreases. Strikingly, regardless of the sample concentration, the observed saturation effects are a signature of an insulating character of the system as far as its relaxation process is concerned. Figure 6(c) presents the  $x$  dependence of the ESR spectra in  $\text{Y}_{1-x}\text{Nd}_x\text{BiPt}$  ( $0.002 \leq x \leq 0.10$ ) at 4.2 K and  $P_{\mu\omega} \approx 5$  mW for  $6.6 \lesssim \lambda \lesssim 30$ . The red solid lines are best fits of the observed spectra to equation (1) using  $1/T_2$  as a fitting parameter and both  $H_1$  and  $T_1$  as constant parameters. The inset to figure 6(c) shows that the linewidth increases

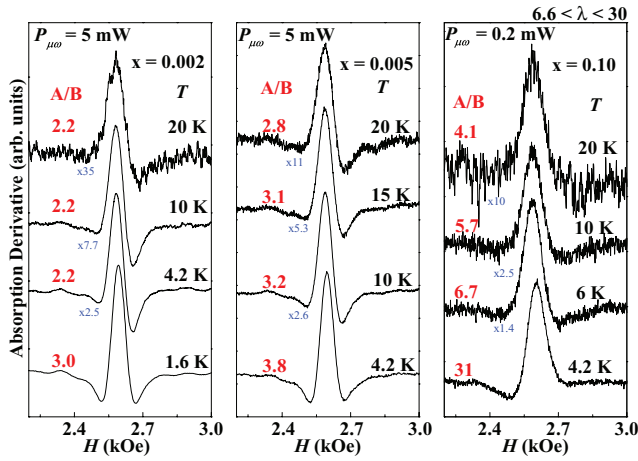


**Figure 5.**  $T$  dependence of the ESR lineshape of  $Y_{1-x}Nd_xBiPt$  with  $6.6 \lesssim \lambda \lesssim 30$  for (a)  $x = 0.002$  at  $P_{\mu\omega} \approx 5$  mW, (b)  $x = 0.005$  at  $P_{\mu\omega} \approx 5$  mW and (c)  $x = 0.10$  at  $P_{\mu\omega} \approx 0.2$  mW. The spectra scaling factors are indicated in blue.

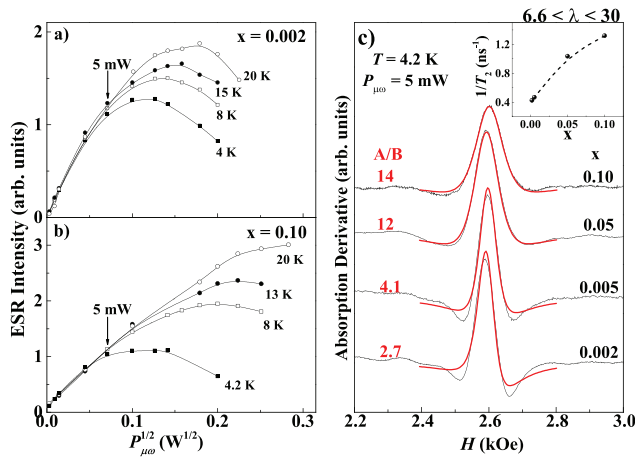


**Figure 6.**  $P_{\mu\omega}$  and  $T$  dependence of the doubly integrated ESR spectra (the double integration procedure is explained in the supplementary information) for  $Y_{1-x}Nd_xBiPt$  and  $6.6 \lesssim \lambda \lesssim 30$  for: (a)  $x = 0.002$  and (b)  $x = 0.10$ . The solid lines are guides to the eyes. (c)  $x$  dependence,  $0.002 \lesssim x \lesssim 0.10$ , of the ESR spectra for  $Y_{1-x}Nd_xBiPt$  at  $T = 4.2$  K,  $P_{\mu\omega} \approx 5$  mW and  $6.6 \lesssim \lambda \lesssim 30$ . Red solid lines are the best fits of the ESR spectra to equation (1) using  $1/T_2$  as a fitting parameter. The inset shows the increase of  $1/T_2$  as  $x$  increases. The solid line is a guide to the eyes.

with the  $Nd^{3+}$  concentration. This is a typical signature for an inhomogeneous broadening due to  $Nd^{3+}-Nd^{3+}$  magnetic interaction. Also, since there is no relaxation via the Korringa mechanism (exchange interaction between  $Nd^{3+}$  and conduction electrons) in  $Y_{1-x}Nd_xBiPt$  [43] the line broadening is expected to be inhomogeneous. Even in the case of a homogeneous thermal broadening (Korringa relaxation) invariably there is still a residual  $T$ -independent linewidth that is inhomogeneous and has different origin such as crystalline defects, chemical disorder induced by doping, spin-spin interaction, etc [50].

Note that a diffusive-like character of the lineshape ( $A/B \gg 2.6 \rightarrow T_D/T_2 \lesssim 1$ ) can be obtained, though fortuitously, using equation (1) for  $s = \gamma^2 H_1^2 T_1 T_2 \gg 1$ . The fittings obtained

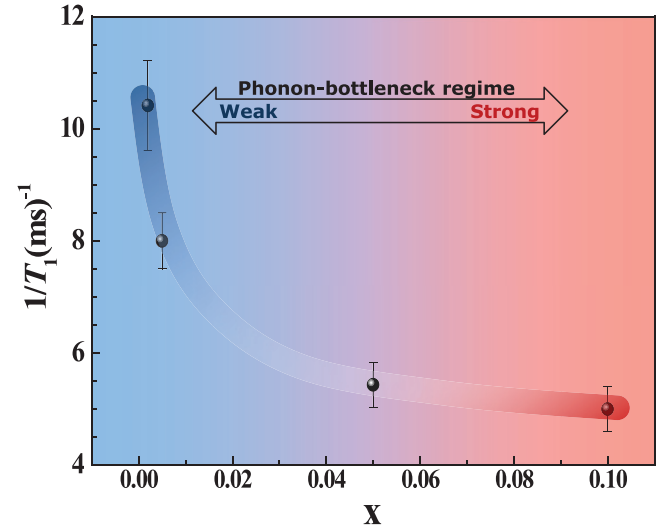


**Figure 7.**  $x$  dependence of  $1/T_1$  of  $Y_{1-x}Nd_xBiPt$  for  $6.6 \lesssim \lambda \lesssim 30$  at  $T = 4.2$  K. The  $1/T_1$  values were obtained from the analysis of the saturation factor [51] of the  $Nd^{3+}$  ESR intensity. The thick solid line is a guide to the eyes.

at low concentration (figure 6(c)) may not seem as good as the others presumably due to the contribution of nonlinear terms at medium and high microwave excitation magnetic field that are not adequately taken into account in this model.

Figure 7 shows the  $x$  dependence of the spin-lattice relaxation rate  $1/T_1$  of  $Y_{1-x}Nd_xBiPt$  with  $6.6 \lesssim \lambda \lesssim 30$  at  $T = 4.2$  K. The spin-spin relaxation time  $T_2$  is obtained directly from the linewidth,  $\Delta H = 1/\gamma T_2$ , at the lowest microwave power level. As for  $T_1$ , it is only possible to estimate its value indirectly from the saturation factor of the doubly integrated ESR spectra,  $I_{sat}/I_{unsat}$  [51]. This limitation is due to the lack of an explicit equation which takes into account the ESR in the high microwave power regime for diffusive processes. Nevertheless, figure 7 shows that  $1/T_1$  slows down systematically as  $x$  increases. This indicates that, as in several other insulators, a *phonon-bottleneck* process dominates the spin-lattice relaxation as the  $Nd^{3+}$  concentration increases in this system [52]<sup>6</sup>.

#### 4. Analysis and discussion

The Dysonian ESR lineshape of diluted  $Gd^{3+}$  and  $Nd^{3+}$  in YBiPt (figure 2), combined with the change of the  $Nd^{3+}$  ESR lineshape with the particle size (figure 3(a)) assure us that these REs are probing the presence of *ce* within the skin depth  $\delta \approx 15 \mu m$ . On the other hand, we have already demonstrated that the spin-lattice relaxation via the exchange coupling between the RE localized magnetic moments and *ce* is very weak in this system. This was the subject of a previous study on crystal field effects of diluted REs ( $Nd^{3+}$ ,  $Gd^{3+}$  and  $Er^{3+}$ )

<sup>6</sup> The *phonon-bottleneck* is characterized by a poor thermal contact between the lattice-phonon reservoir and the thermal bath (Kapitza resistance), confining the energy absorbed at resonance by the local moments to be back and forth, via SO coupling, between the localized magnetic moments and lattice-phonons. As such, higher local moment concentration will lead to stronger confinement.

in  $Y_{1-x}RE_xBiPt$  [42, 43]. This conclusion was drawn mainly based on the very small thermal broadening of the ESR linewidth (Korringa relaxation rates) along with the negligible  $g$ -shifts (Knight shifts) measured for these REs [43]<sup>7</sup>. These findings were also corroborated by the small Sommerfeld coefficient ( $\gamma \lesssim 0.1$  mJ molK<sup>-1</sup>) found in this material [43]. They are all quite consistent with the small gap ( $\Delta \approx 0.1 - 0.01$  eV) reported for YBiPt [33, 34, 42, 43].

Thus, the relaxation of localized magnetic moments to the thermal bath should be mainly processed throughout the lattice phonons via their own SO coupling ( $\lambda_{4f}L_{Nd} \cdot S_{Nd}$ ) [52] as is the case of any insulator in the diluted limit and not by the exchange interaction with  $ce$  ( $(g_j - 1)J_{fs}J_{Nd} \cdot s_{ce}$ ) as usually occurs in metallic hosts [53].

As such, in spite of the observed metallic (Dysonian-like) ESR lineshapes [45, 47] displayed in figures 3–6, the low- $T$  ESR linewidth of diluted REs in YBiPt is expected to be inhomogeneous (see figure 6(c)) and the spin–spin relaxation time much shorter than the spin-lattice relaxation time ( $T_2 \ll T_1$ ) as observed for any conventional insulator. Moreover, figures 6(a) and (b) show that the Nd<sup>3+</sup> ESR intensity saturates for  $T \lesssim 20$  K and  $P_{\mu\omega} \gtrsim 5$  mW, confirming the slow spin-lattice relaxation rate  $1/T_1$ . A direct conclusion is that the relaxation process is actually driven by phonons via SO coupling. This result combined with the particle size (figure 3(a)), microwave power (figures 3(b) and 4(a)–(c)), temperature (figures 5(a)–(c)) and concentration (figure 6(c)) dependencies of the Nd<sup>3+</sup> ( $\Gamma_6$  Kramers' doublet;  $S_{\text{eff}} = 1/2$ ) ESR lineshape indubitably assure us that insulating and metallic behaviors coexist within the skin depth ( $\delta \approx 15$   $\mu\text{m}$ ) of YBiPt.

Now, for the ESR spectral analysis we shall go back to equation (1). It is worth noting that the phenomenological lineshape analysis used here must be taken with caution. In this approach, we incorporated the saturation term  $s = \gamma^2 H_1^2 T_2 T_1$  into the admixture of absorption and dispersion to fully explain the lineshape changes and take into account the spin-lattice relaxation time  $1/T_1$  from the corresponding ESR saturation data. It is possible that this procedure may not capture all details related with the complex phenomenon involving the process of resonant microwave absorption diffusing to the thermal bath in the presence of a *phonon-bottleneck* process, which is further discussed below.

Figure 8(a) shows the simulations of the data of figures 3(b) and 4(b) using equation (1). The spin–spin,  $1/T_2$ , and spin-lattice,  $1/T_1$ , relaxation rates were kept constant. The simulated spectra show that the ESR lineshape changes from a diffusionless to a greatly diffusive-like regime as  $P_{\mu\omega}$  increases. Despite a small broadening, these simulations reproduce the general lineshape features presented in figures 3(b) and 4(b) reasonably well. However, in order to eliminate this extra broadening, which is not observed experimentally, we forced the narrowing of the linewidth  $\Delta H = 1/\gamma T_2$  as  $P_{\mu\omega}$  increases

<sup>7</sup> The  $g$ -value is obtained from best fits of the Nd<sup>3+</sup> spectra to equation (1) at low microwave power, where saturation effects are negligible. So, at a low microwave power limit the saturation term can be neglected. Using  $H_0 = h\nu/g\mu_B$  we obtain  $g$ -value,  $g = 2.66(4)$  ( $g$ -value in insulator), indicating no  $g$ -shift. [39], p 876.

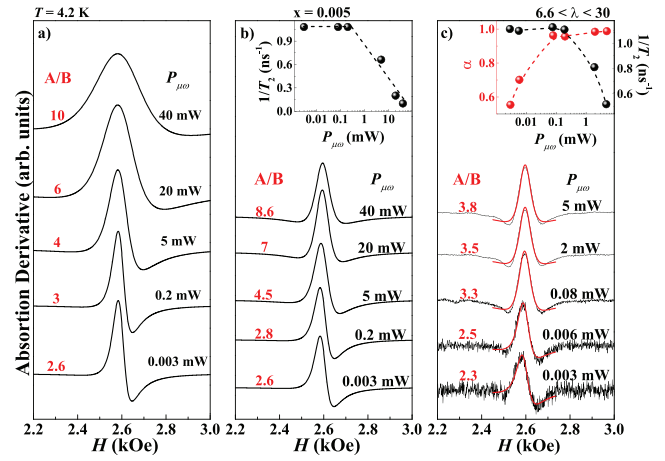


**Figure 8.** Theoretical  $P_{\mu\omega}$  dependence (equation (1)) of the ESR lineshape of  $Y_{0.995}Nd_{0.005}BiPt$  for  $6.6 \lesssim \lambda \lesssim 30$  at  $T = 4.2$  K; (a) simulations with constant  $1/T_2$  and  $1/T_1$ ; (b) simulations with  $1/T_1$  constant and  $1/T_2$  following the  $P_{\mu\omega}$  dependence (logarithmic scale) shown in the inset; and (c) the red lines are fits of the data of figure 4(b) with equation (1) with constant  $1/T_1$ . The extracted parameters of absorption/dispersion admixture,  $\alpha$ , and  $1/T_2$  are shown in the inset. The solid lines are guides to the eyes.

keeping  $1/T_1$  constant. The result is presented in figure 8(b) which displays the simulated spectra for the ESR data of figure 4(b). The inset to figure 8(b) shows the extracted phenomenological  $P_{\mu\omega}$  dependence of  $1/\gamma T_2$ . Notice that the narrowing of the linewidth begins around  $P_{\mu\omega} \approx 5$  mW where the resonance starts to saturate (*non-thermal equilibrium*) (see figures 6(a) and (b)). From this point on, an exponential behavior is obtained for the spin–spin relaxation rate,  $1/T_2 \sim e^{-aP_{\mu\omega}}$ , where  $a$  is a fitting parameter. The decrease of  $\Delta H$  with  $P_{\mu\omega}$  can be ascribed as a reduction of  $1/T_2$  due to an evanescent local fluctuating field (*secular* and *non-secular* broadenings) [54] caused by the saturation of the ensemble of the Nd<sup>3+</sup> ions.

Nonetheless, we believe that our most important and remarkable experimental result is the dramatic change of the Nd<sup>3+</sup> ESR lineshape from a diffusionless ( $A/B \approx 2.6$ ;  $T_D/T_2 \gg 1$ ) to a diffusive regime ( $A/B \gtrsim 2.6 \rightarrow T_D/T_2 \lesssim 1$ ) observed for  $P_{\mu\omega} \lesssim 200$   $\mu\text{W}$  and  $T \lesssim 10$  K. This behavior is clearly seen in the size (figure 3(a)),  $P_{\mu\omega}$  (figures 3(b) and 4(b)) and  $T$  dependence (figures 5(a)–(c)) of the ESR spectra. For the dependence with  $P_{\mu\omega}$  shown in figure 4(b), the ESR spectra display a drastic lineshape change well below  $\approx 5$  mW, which is the microwave power limit above which saturation effects begin to be observed (figures 6(a) and (b)). Besides, this drastic lineshape change is revealed by our simulated spectra only at  $P_{\mu\omega} \geq 20$  mW (see figure 8(a)). It occurs below  $\approx 200$   $\mu\text{W}$  and  $\approx 80$   $\mu\text{W}$ , respectively, for the samples of figures 3(b) and 4(b) (also for the sample with  $x = 0.05$ , not shown). Therefore, we conclude that the lineshape change for  $P_{\mu\omega} \lesssim 200$   $\mu\text{W}$  is unrelated to the saturation phenomenon.

Hence, the  $\alpha$  parameter (admixture of absorption/dispersion) in equation (1) was phenomenologically adjusted in the limit of low- $P_{\mu\omega}$  to fit the data of figure 4(b). The best fits are presented in figure 8(c). The  $P_{\mu\omega}$  dependence of  $\alpha$  is shown in the inset of figure 8(c). Note that the fits are not quite able

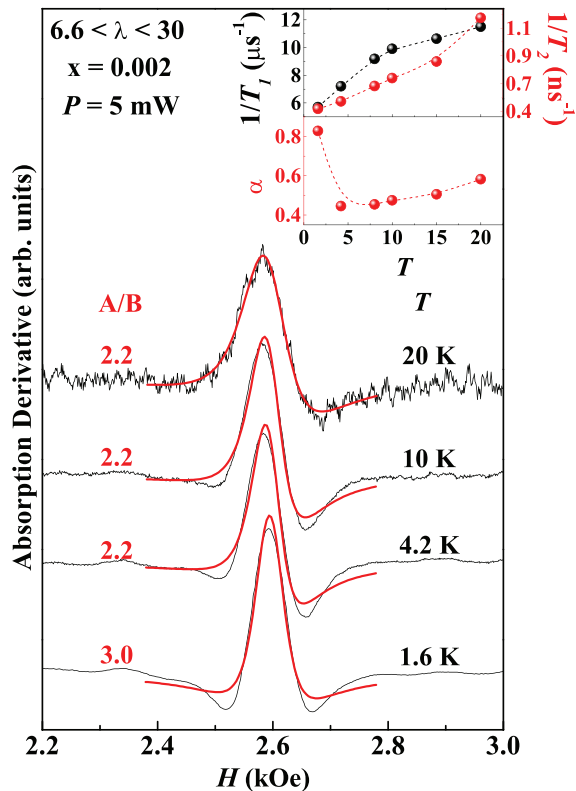


**Figure 9.** The red lines represent fittings to equation (1) of the  $T$  dependence ESR lineshape for  $\text{Y}_{0.998}\text{Nd}_{0.002}\text{BiPt}$  for  $6.6 \lesssim \lambda \lesssim 30$  and  $P_{\mu\omega} \approx 5$  mW. The spin–spin relaxation rate,  $1/T_2$ , and  $\alpha$  are variable fitting parameters.  $\alpha$  is the admixture parameter of absorption ( $\alpha = 0$ ) and dispersion ( $\alpha = 1$ ). The spin-lattice relaxation rate,  $1/T_1$ , was obtained from the saturation data of figure 5(a). Their  $T$  dependence are shown in the inset. The dashed lines are guides to the eyes.

to reproduce the two lateral wings of the resonance although they do capture the overall observed lineshape changes at the same  $P_{\mu\omega}$  ( $\approx 100 \mu\text{W}$ ). This  $P_{\mu\omega}$  is well below the regime where the saturation effects start to set in ( $\approx 5$  mW). The inability of the fits to exactly reproduce the experimental spectra may be due to the simplistic phenomenological approach.

Regarding the  $T$ -dependent ESR lineshape of figure 5(a), we show in figure 9 the best fits of the spectra to equation (1).  $T_2$  and  $\alpha$  were taken as variable parameters and  $T_1$  was estimated from the saturation factors [51] of figure 6(a). The obtained  $T$  dependences of  $1/T_2$ ,  $1/T_1$  and  $\alpha$  are shown in the inset to figure 9. These results show that both  $1/T_1$  and  $1/T_2$  rates increase as  $T$  increases, restoring the diffusionless lineshape and the local fluctuating field as the ensemble of  $\text{Nd}^{3+}$  ions reaches its thermal equilibrium (unsaturated state). In other words, the increasing presence of phonons as  $T$  is increased restores the thermodynamic equilibrium conditions. At this point, it is worth mentioning that evidence for *ce-phonon* interaction has also been visualized in the optical properties of Bi-based TIs, where *ce-phonon* coupling suppresses the surface conducting states as the temperature rises [55].

Now, let us focus on the striking result shown in figure 7: the  $\text{Nd}^{3+}$  spin-lattice relaxation rate decreases as the  $\text{Nd}^{3+}$  concentration increases. This is an indication that the  $\text{Nd}^{3+}$

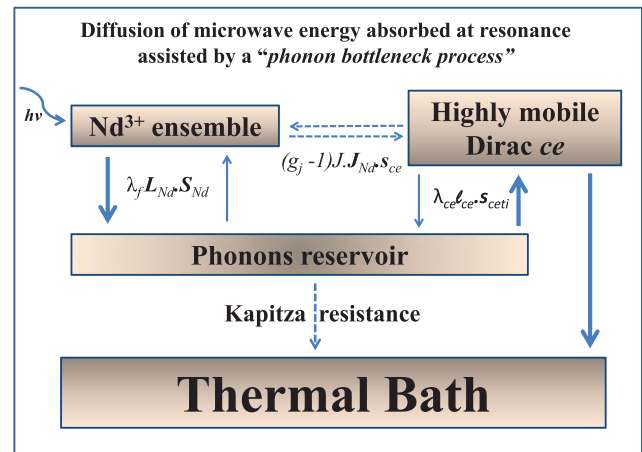


**Figure 10.** Illustrative route diagram for the diffusion of the microwave energy absorbed at resonance to the thermal bath (thick solid blue arrows) assisted by the *phonon-bottleneck process*. The blue dashed arrows indicate weak coupling mechanism.

relaxation process is driven by the *phonon-bottleneck phenomenon* in the high  $\text{Nd}^{3+}$  concentration limit. This allow us to conclude that the phonons are poorly connected to the thermal bath which may indicate relatively high Kapitza resistance [56] in  $\text{YBiPt}$ . Therefore, we suggest that the smooth change of the lineshape from diffusionless ( $\alpha \approx 0.5 \rightarrow T_D/T_2 \gtrsim 1$ ) to diffusive ( $\alpha \approx 1 \rightarrow T_D/T_2 \lesssim 1$ ) between  $\approx 2 \mu\text{W}$  and  $\approx 100 \mu\text{W}$  (figures 3(b) and 4(b)) and for  $T \lesssim 10$  K (figures 5(a)–(c)) within the skin depth  $\delta \approx 15 \mu\text{m}$  is associated with the development of a *long lifetime phonon reservoir* due to the poor phonon-thermal bath contact. We argue that these *long lifetime phonons* could excite highly mobile *ce* within the skin depth of this TNSM compound via *ce-phonon* SO coupling, since the *ce* SO coupling ( $\lambda_{ce} l_{ce} \cdot s_{ce}$ ) is an important ingredient for the TNSM [6–8]. Thereby, these highly mobile *ce* would be able to diffuse across the skin depth and deliver the microwave energy absorbed at resonance by the  $\text{Nd}^{3+}$  ions to the thermal bath. Thus, the coupling between *long lifetime phonons* and highly mobile *ce* within the skin depth would be playing the same role as diffusing *ce* across the skin depth in conventional conduction electron spin resonance (CESR) in normal metals as described by Dyson’s theory [47]. In other words, Dyson’s theory is concerned with the microwave energy absorbed at resonance by a spin system within the skin depth. Now, if the spin system diffuses across the skin depth in a time shorter than the spin lattice relaxation time, as may happen in the case of *ce*, what is actually and effectively diffusing across the skin depth is the microwave energy absorbed at resonance carried on by the *ce*. Therefore, in the case of the  $\text{Nd}^{3+}$  ESR in  $\text{YBiPt}$ , in spite of the fact that they are localized in the lattice, what is actually diffusing across the skin depth is the microwave energy absorbed at resonance. The illustrative route diagram presented in figure 10 shows a plausible path, represented by the thick solid (blue) arrows, for the flow of the net microwave energy absorbed at resonance finally reaching the thermal bath via our proposed *phonon-bottleneck process*.

The intriguing results of figure 3(a) for the sample in the strong *phonon-bottleneck* regime ( $x = 0.10$ ) at low- $P_{\mu\omega}$  clearly



show a diffusionless lineshape for large particles and diffusive for the small ones. As seen, such results can be predicted by adjusting the  $\alpha$  parameter in equation (1) as shown in figures 8(c) and 9. Notice though that even for the smallest studied particle size, their dimensions are still several times larger than the skin depth. We believe that the observed lineshape change is related to the surface/volume ratio which is enhanced as the particle size is decreased. This would favor surface distortions which in turn increase the metallic states within the skin depth of this TNSM compound [16, 19, 29–31] and improve the energy transfer process: *long lifetime phonons*  $\rightarrow$  *highly mobile ce*  $\rightarrow$  *thermal bath*. Hence, smaller particle size tends to improve the diffusion of the microwave energy absorbed at resonance by the  $\text{Nd}^{3+}$  ions to the thermal bath.

Furthermore, by considering  $T_2 \approx 10^{-9}$  s at low power  $P_{\mu\omega} \approx 0.002$  mW and knowing that  $A/B \approx 14 \rightarrow T_D/T_2 \approx 0.02$  at  $P_{\mu\omega} \approx 0.2$  mW (see figure 3(b)), the diffusion time  $T_D \approx 2 \times 10^{-11}$  sec can be estimated for the highly mobile *ce* within the strong *phonon-bottleneck* regime.

It is worth discussing the estimated  $T_D$  value enlightened by the intrinsic transport parameters of YBiPt. A carrier density of  $n \cong 1.7 \times 10^{18}$   $\text{cm}^{-3}$  and an electron effective mass  $m^* \cong 0.15m_0$  can be obtained from Shubnikov–de Haas measurements at 0.1 K and the  $T$  dependence of the amplitude of the oscillations, respectively, assuming a spherical Fermi surface [34]. From the relation  $\rho = m^*/e^2n\tau$  and using the low- $T$  resistivity  $\rho \cong 0.7$   $\text{m}\Omega\text{cm}$  [34] we estimate the *ce* Coulomb-type collision mean time  $\tau \cong 4.48 \times 10^{-13}$  s. Thus, a mobility of about 5200  $\text{cm}^2 \text{Vs}^{-1}$  which is the order of the Hall mobility [34] can be predicted by considering  $\mu = e\tau/m^*$ . Hence, from the ratio  $T_D/\tau \approx 44$  we estimate that the *ce* experience one spin-flip scattering after approximately 50 Coulomb-type collisions. Besides, the Fermi velocity  $v_F \approx 3 \times 10^5$   $\text{m s}^{-1}$  can be also obtained from the mean free path  $l = v_F\tau$  with  $l = \hbar k_F/\rho ne^2 \approx 128$  nm and  $k_F = [3\pi^2n]^{1/3} \approx 3.7 \times 10^8$   $\text{m}^{-1}$ . Therefore, a *ce* carrying the energy absorbed at resonance by the  $\text{Nd}^{3+}$  ions may travel a distance of  $\approx 6$   $\mu\text{m}$  before a spin-flip scattering occurs. This length is comparable with the skin depth  $\delta \approx 15$   $\mu\text{m}$  estimated for  $\text{Y}_{1-x}\text{Nd}_x\text{BiPt}$  and, thus, explains the diffusive lineshape observed by the localized  $\text{Nd}^{3+}$  in our ESR experiments.

It is also worth mentioning that the microwave photons with energy  $h\nu/k_B \approx 0.5$  K may promote electrons across subtly gapped Dirac cones near the sample surface. Thus, the density of *ce* might increase on the surface of the material with increasing microwave power. As a consequence, the surface conductivity would also increase, affecting the skin depth and favoring the diffusion of the microwave energy absorbed at resonance by the  $\text{Nd}^{3+}$  ions to the thermal bath. This *ce* activation can only be induced by electric dipolar transitions associated with the electric component of the applied microwave [57]. Nonetheless, this may not be relevant here since the sample is located at the minimum microwave electric field inside the  $\text{TE}_{102}$  ESR resonator (cavity) used in our ESR experiments.

Additionally, we should report that a similar study has been performed on  $\text{Y}_{1-x}\text{Gd}_x\text{BiPt}$  for  $0.01 \lesssim x \lesssim 0.05$ . Saturation

effects at low  $T$  and high microwave power ( $P_{\mu\omega} \approx 100$  mW) were also observed, but with an inexpressive phonon-bottleneck effect and much less pronounced changes in the lineshape as a function of  $\text{Gd}^{3+}$  concentration and microwave power when compared with  $\text{Y}_{1-x}\text{Nd}_x\text{BiPt}$  ( $\text{Nd}^{3+}$ : non  $S$ -state,  $L \neq 0$ ;  $S_{\text{eff}} = 1/2$ , two-fold ground state multiplet). The relaxation process due to phonons via spin–orbit coupling is expected to be very different for an  $S$ -state ion as  $\text{Gd}^{3+}$  if compared with a non- $S$  ion as  $\text{Nd}^{3+}$ . The resulting  $\text{Gd}^{3+}$  ESR spectrum consists of seven crystal field unresolved ESR transitions ( $S_{\text{eff}} = 7/2$ ) and, therefore, the  $\text{Gd}^{3+}$  ions are expected to be less susceptible to the phonon-bottleneck relaxation process than in a non- $S$  ion such as  $\text{Nd}^{3+}$  ( $S_{\text{eff}} = 1/2$ ) [52]. The spin-lattice relaxation time throughout seven channels is certainly very different than that of  $\text{Nd}^{3+}$ . We attribute the remarkable difference between the  $\text{Nd}^{3+}$  and  $\text{Gd}^{3+}$  lineshapes to a weakly concentration dependent spin-lattice relaxation of  $\text{Gd}^{3+}$  ions in YBiPt (not shown) indicating that there is no or less pronounced phonon-bottleneck effect in this case. As mentioned above, the phonon-bottleneck process is crucial for the diffusive effect of  $\text{Nd}^{3+}$ . Besides, the  $\text{Gd}^{3+}$  resonance was obtained under exactly the same experimental conditions of matching, tuning and AFC as for the  $\text{Nd}^{3+}$  + diffusive-like lineshape. Therefore, lineshape distortions due to extrinsic dispersive effects would be very unlikely.

## 5. Conclusions

The systematic ESR study of the  $\text{Nd}^{3+}$   $T_6$  Kramers' doublet ( $S_{\text{eff}} = 1/2$ ) CEF ground state in the cubic non-centrosymmetric half Heusler semiconductor/semimetallic compound  $\text{Y}_{1-x}\text{Nd}_x\text{BiPt}$  revealed that this system presents, simultaneously, metallic and insulating features within the skin depth. This dual character was verified by the saturation effects and relaxation processes observed on the Dysonian (metallic lineshape) of the  $\text{Nd}^{3+}$  ESR spectra. Also, our phenomenological analysis of the the ESR lineshape suggests that saturation effects do affect the local fluctuation field and contribute to slowing down the effective spin–spin relaxation rate,  $1/T_2$ , i.e. narrowing down the inhomogeneous ESR linewidth.

Moreover, the dramatic evolution of the lineshape between diffusionless ( $A/B \lesssim 2.6 \rightarrow T_D/T_2 \gg 1$ ) and diffusive regimes ( $A/B \gtrsim 2.6 \rightarrow T_D/T_2 \lesssim 1$ ) in the absence of saturation effects ( $P_{\mu\omega} \lesssim 200$   $\mu\text{W}$ ), strongly suggests that this peculiar behavior is caused by a subtle combination between the increasing presence of the *phonon-bottleneck* process (as the  $\text{Nd}^{3+}$  concentration increases) and the highly mobile *ce* in this tunable topologically nontrivial semimetal.

In conclusion, the *phonon-bottleneck* process allowed us to observe the striking diffusive effect on the  $\text{Nd}^{3+}$  ESR metallic lineshape in YBiPt. We argue that, within the skin depth ( $\delta \approx 15$   $\mu\text{m}$ ), the *phonon-bottleneck* process yields a *long lifetime phonon reservoir* where the *ce*-phonon SO coupling permits highly mobile *ce* at the Fermi level, carrying microwave energy absorbed at resonance by the  $\text{Nd}^{3+}$  ions, diffuses it across the skin depth and, finally, deliver it to the thermal bath.

## Acknowledgments

We are thankful to Y Kopelevich for enlightening discussions. This work was conducted under the auspices of FAPESP (Grant Nos. 2006/60440-0, 2007/50986-0, 2011/01564-0, 2012/05903-6), CNPq, FINEP and CAPES (Brazil), and NSF (DMR-0801253) (USA).

## References

- [1] Qi X-L and Zhang S-C 2010 *Phys. Today* **63** 33
- [2] Hasan M Z and Kane C L 2010 *Rev. Mod. Phys.* **82** 3045
- [3] Moore J E 2010 *Nature* **464** 194
- [4] Qi X-L and Zhang S-C 2011 *Rev. Mod. Phys.* **83** 1057
- [5] Culcer D 2012 *Physica E* **44** 860
- [6] Moore J E and Balents L 2007 *Phys. Rev. B* **75** 121306
- [7] Fu L, Kane C L and Mele E J 2007 *Phys. Rev. Lett.* **98** 106803
- [8] Roy R 2009 *Phys. Rev. B* **79** 195322
- [9] Bernevig B A, Hughes T L and Zhang S-C 2006 *Science* **314** 1757
- [10] Konig M, Wiedmann S, Brune C, Roth A, Buhmann H, Molenkamp L W, Qi X-L and Zhang S-Q 2007 *Science* **318** 766
- [11] Fu L and Kane C L 2007 *Phys. Rev. B* **76** 045302
- [12] Hsieh D, Quian D, Wray L, Xia Y, Hor Y, Cava R J and Hasan M Z 2008 *Nature* **452** 970
- [13] Zhang H *et al* 2009 *Nat. Phys.* **5** 438
- [14] Xia Y *et al* 2009 *Nat. Phys.* **5** 398
- [15] Chen Y L *et al* 2009 *Science* **325** 178
- [16] Fu L 2011 *Phys. Rev. Lett.* **106** 106802
- [17] Dziawa P *et al* 2012 *Nat. Mater.* **11** 1023
- [18] Hsieh T H, Lin H, Liu J, Duan W, Bansil A and Fu L 2012 *Nat. Commun.* **3** 982
- [19] Chadov S, Qi X-L, Keubler J, Fecher G H, Felser C and Zhang S-C 2010 *Nat. Mater.* **9** 541
- [20] Dzero M, Sun K, Galitski V and Coleman P 2010 *Phys. Rev. Lett.* **104** 106408
- [21] Fisk Z *et al* 1991 *Phys. Rev. Lett.* **67** 3310
- [22] Kim D J, Grant T and Fisk Z 2012 *Phys. Rev. Lett.* **109** 096601
- [23] Kim D J, Thomas S, Grant T, Botimer J, Fisk Z and Xia J 2013 *Sci. Rep.* **3** 3150
- [24] Wolgast S, Kurdak C, Sun K, Allen J W, Kim D-J and Fisk Z 2013 *Phys. Rev. B* **88** 180405
- [25] Neupane M *et al* 2013 *Nat. Commun.* **4** 2991
- [26] Jiang J *et al* 2013 *Nat. Commun.* **4** 3010
- [27] Kim D J, Xia J and Fisk Z 2014 *Nat. Mater.* **13** 466
- [28] Zhou Y *et al* 2015 *Phys. Rev. B* **92** 241118(R)
- [29] Zeljkovic I *et al* 2015 *Nat. Mater.* **14** 318
- [30] Sun K 2015 *Nat. Mater.* **14** 262
- [31] Lin H, Wray L A, Xia Y, Xu S, Cava R J, Bansil A and Hasan M Z 2010 *Nat. Mater.* **9** 546
- [32] Xiao D, Yao Y, Feng W, Wen J, Zhu W, Chen X-Q, Stocks G M and Zhang Z 2010 *Phys. Rev. Lett.* **105** 096404
- [33] Canfield P C, Thompson J D, Beyermann W P, Lacerda A, Hundley M F, Peterson E, Fisk Z and Ott H R 1991 *J. Appl. Phys.* **70** 5800
- [34] Butch N P, Syers P, Kirshenbaum K, Hope A P and Paglione J 2011 *Phys. Rev. B* **84** 220504
- [35] Pagliuso P G, Baumbach R, Rosa P F S, Adriano C, Thompson J D and Fisk Z 2013 Low temperature specific heat of YBiPt *APS March Meeting (Baltimore, Maryland, 18–22 March 2013) (Bulletin of the American Physical Society vol 58)* (College Park, MD: American Physical Society) **B13.00013**
- [36] Shekhar C *et al* 2015 arXiv:1502.00604
- [37] Bauer E and Sigrist M (ed) 2012 *Non-Centrosymmetric Superconductors (Lecture Notes in Physics vol 847)* (Berlin: Springer)
- [38] Schnyder A P, Brydon P M R and Timm C 2012 *Phys. Rev. B* **85** 024522
- [39] Abragam A and Bleaney B 1970 *Electron Paramagnetic Resonance of Transition Ions* (Oxford: Clarendon)
- [40] Taylor R H 1975 *Adv. Phys.* **24** 681
- [41] Barnes S E 1981 *Adv. Phys.* **30** 801
- [42] Martins G B, Rao D, Barberis G E, Rettori C, Duro R J, Sarrao J, Fisk Z, Oseroff S and Thompson J D 1995 *Phys. Rev. B* **52** 15062
- [43] Pagliuso P G, Rettori C, Torelli M E, Martins G B, Fisk Z, Sarrao J L, Hundley M F and Oseroff S B 1999 *Phys. Rev. B* **60** 4176  
Güner S, Rameev B and Aktas B 2003 *J. Magn. Magn. Mater.* **258–9** 372–5
- [44] Canfield P C and Fisk Z 1992 *Phil. Mag.* **65** 1117
- [45] Feher G and Kip A F 1955 *Phys. Rev.* **98** 337
- [46] Bowan M K, Hase H and Kevan L 1976 *J. Magn. Res.* **22** 23
- [47] Dyson F J 1955 *Phys. Rev.* **98** 349
- [48] Kaplan J I 1959 *Phys. Rev.* **115** 575
- [49] Pake G E and Purcell E M 1948 *Phys. Rev.* **74** 1184
- [50] Cabrera-Baez M, Iwamoto W, Magnavita E T, Osorio-Guillen J M, Ribeiro R A, Avila M A and Rettori C 2014 *J. Phys.: Condens. Matter* **26** 17
- [51] Poole C P Jr 1969 *Electron Spin Resonance, a Comprehensive Treatise on Experimental Techniques* (New York: Interscience) pp 705–17
- [52] Orbach R L 1961 *Proc. R. Soc.* **264** 458  
Standley K J and Vaughan R A 1969 *Electron Spin Relaxation in Solids* (New York: Plenum) pp 62–74
- [53] Rettori C, Davidov D, Orbach R and Chock E P 1973 *Phys. Rev. B* **7** 1  
Rettori C, Oseroff S B, Rao D, Pagliuso P G, Barberis G E, Sarrao J, Fisk Z and Hundley M 1997 *Phys. Rev. B* **55** 1016
- [54] Slichter C P 1963 *Principles of Magnetic Resonance* (New York: Harper & Row) pp 148–56
- [55] Reijnders A A 2014 *Phys. Rev. B* **89** 075138
- [56] Cheeke J D N 1970 *J. Physique Colloq.* **31** C3-129
- [57] Lindner N H, Refael G and Galitski V 2011 *Nat. Phys.* **7** 490